

Electrodeposition of Fe-Sn from the chloride-based electrolyte

Simona Mrkonjić Zajkoska*^{1,2}, Rudolf Mann¹, Wolfgang Hansal*¹,
Sudipta Roy³, Wolfgang Kautek²

¹ *Hirtenberger Engineered Surfaces GmbH, Hirtenberg, Austria*

² *Department of Physical Chemistry, University of Vienna, Vienna, Austria*

³ *Chemical and Process Engineering Department, University of Strathclyde, Glasgow,
United Kingdom*

*Corresponding authors: simona.zajkoska@hirtenberger.com,
wolfgang.hansal@hirtenberger.com*

Electrodeposition of Fe-Sn alloys from a chloride-based electrolyte

The conditions for electrodeposition of Fe-Sn alloys from a novel, environmentally friendly, ferrous chloride-based electrolyte were studied. The influence of the pH on the electrolyte stability and deposit stoichiometry was discussed. Anodic stripping voltammetry (ASV), XRD and SEM/EDX were used to characterize the electrodeposited phases. The results from ASVs indicated the possibility to deposit at least two different phases at high overpotentials. Hull cell depositions in an electrolyte with a Sn to Fe ratio 1:1 and a pH value of 2.8 showed regular deposition of Fe-Sn. Fe-rich deposits (54.84 at %) were obtained from an electrolyte with Sn to Fe ratio 1:10. The XRD results were compatible with the electrochemical investigations. In all studied samples β -Sn, FeSn₂ and Fe₅Sn₃ were detected. The presence of ferromagnetic Fe₅Sn₃ was not influenced by the Sn to Fe ions ratio in the electrolyte.

Keywords: tin-iron electrodeposition; ferrous-stannous electrolyte; anodic stripping voltammetry; Hull cell; chloride; XRD

Introduction

Nowadays, the alloys used most frequently for magnetic materials are iron based with nickel and cobalt [1]. However, Ni is highly allergenic and Co(II) salts are carcinogenic and materials of very high concern according to European Chemicals Agency [2]. Fe-Sn alloys are a potential alternative to these classical magnetic materials. In the binary thermal equilibrium diagram of Fe-Sn five intermetallic compounds are found, namely: FeSn₂, FeSn, Fe₃Sn₂, Fe₅Sn₃ and Fe₃Sn [3]. The iron-rich compounds Fe₃Sn₂, Fe₅Sn₃ and Fe₃Sn are ferromagnetic [3] and, due to their low cost and low harm to health and environment, interesting for industrial usage. Possible applications of the Fe-Sn alloy deposits are magnetic recording [4,5] or corrosion protection coatings [6]. Different Fe-Sn phases were obtained by mechanical milling [7], alloying [8] or co-sputtering [9,10]. Literature research showed almost no records in the field of

electrodeposition of Fe-Sn [11].

In our previous research we were studying the mechanism of electrodeposition of Fe-Sn from ferric salts and tartrate as a single complexing agent [12]. However, the electrochemical equivalent of Fe^{3+} is lower than the one of Fe^{2+} . Therefore, in the present study, the conditions for Fe-Sn electrodeposition from a ferrous, chloride based electrolyte are discussed. Influence of the pH and Sn-Fe ion ratio in the electrolyte on the deposit morphology and stoichiometry is described. Anodic stripping was used to characterize the possible electrodeposited phases of Fe-Sn. In all the deposited samples a ferromagnetic Fe_5Sn_3 was detected.

Materials and Methods

The conditions of co-deposition of Fe-Sn were studied in a chloride-based electrolyte (

Table 1). Electrochemical experiments were carried out in a standard 300 ml electrochemical cell with a three electrodes setup. The working electrode was a gold tipped rotating disc electrode (RDE, 0.1 cm radius). A platinum wire was used as a counter electrode. A saturated calomel electrode (SCE), connected via a Luggin capillary, was used as a reference electrode. In the text all the potentials were recalculated to the standard hydrogen electrode (SHE) as a reference. The electrolyte temperature was kept constant at 60°C with a water bath. All the experiments were carried out using an μ Autolab II (Metrohm) potentiostat, controlled with the NOVA 2.0 software. The surface of the RDE was wet polished with 4000 grid silicon paper and washed with DI water before each experiment. Electrolyte pH was adjusted with 10% H₂SO₄.

Table 1: Electrolyte composition. Metal ion concentration (Sn + Fe) was kept constant at 0.11 M with different Sn:Fe ion ratio.

3Na citrate x 2H ₂ O (Sigma Aldrich)	0.27 M
KNa tartrate x 4H ₂ O (Sigma Aldrich)	0.09 M
(NH ₄) ₂ SO ₄ (Sigma Aldrich)	0.45 M
SnCl ₂ x2H ₂ O (Sigma Aldrich)	
FeCl ₂ x 4H ₂ O (Alfa Aesar)	

The deposition potential of Sn was measured from an electrolyte containing only 0.11 M of Sn as an electroactive substance. Polarization measurements for this electrolyte were performed on a static RDE with a scan rate of 5 mV/s, starting at the OCP and continued into the cathodic direction until -1.25 V vs. SHE. Anodic stripping voltammograms (ASVs) in the single metal Sn electrolyte were carried out at the pH value that has been present in the electrolyte initially and it has not been further adjusted.

The deposition potential of Fe in a chloride-based electrolyte was determined in an electrolyte containing 0.11 M of Fe as an electroactive species. Since hydrogen evolution is a significant side reaction of Fe deposition, the reduction potential of Fe could not be determined directly. For this purpose, a series of ASVs with the scan rate of 30 mV/s were carried out. Fe was electrodeposited during the cathodic polarisation sweep. The cathodic reverse potential was varied from -0.35 V to -1.25 V vs. SHE with the step of -0.1 V. . The appearance of the Fe anodic stripping peak indicated the position of the Fe reduction potential. The measurements were first carried out in an electrolyte with non-adjusted pH with the value of 6.0 and afterwards at a pH of 2.8.

Anodic stripping voltammetry as an in-situ technique for characterization of electrodeposited Fe-Sn layers was used. Electrodeposition of the layers was performed via cathodic polarization of the stationary, gold disc electrode. Electrolytes with Sn to Fe ratio 1:1, 1:3 and 1:10 were tested at the pH of 2.8. In the electrolyte with Sn to Fe ratio 1:3 the cathodic potential was changed from -0.95, -1.05 to -1.25 V. Current density transients were recorded on a gold tipped RDE at the potential -0.75 V vs SHE with 100 rpm for 300 s.

The metal speciation was calculated in Visual MINTEQ 3.1 [13]. The oxidation of Fe^{2+} to Fe^{3+} was not considered in the chemical equilibrium modelling. Consequently, Hyperquad Simulation and Speciation (HySS) software [14] was used for the calculation of species' concentration and visualization.

Galvanostatic Fe-Sn deposits were obtained from Hull cell experiments which were carried out in a standard 267 ml cell (Kocour). A constant current of 1 A was applied for 10 minutes on a brass substrate. For this purpose, electrolytes (pH~2.8) with Sn to Fe ion ratios 1:1 and 1:10 were prepared. Attempts to achieve smoother deposits from the Sn:Fe electrolyte 1:10 were made by adding 1.6 mg/l of alkoxyated β -naphthol [15] (ABN). The electrodeposited dendrites were collected on a double side adhesive carbon tape and investigated with SEM/EDX. In order to study the phase composition and overall stoichiometry of the compact underlying layer, the dendrites were mechanically removed by rubbing with an isopropanol wetted cotton pad. The SEM/EDX investigation was performed on the 1x1 cm sample cut along the 40 mA/cm^2 zone of the Hull cell electrode. In the nominal current densities the SEM/EDX samples were cut between 33.78 and 48.44 mAcm^{-2} [16].

The surface topography and the deposit stoichiometry were analysed with the scanning electron microscope (SEM) Hitachi S-4800 equipped with an energy dispersive

X-ray detector (EDX). The phase composition of the deposits was studied with an X-ray diffractometer Empyrean PANalytical using a grazing incidence geometry. The samples were scanned at $10\text{-}100^\circ$ 2θ with $\text{CuK}\alpha$ radiation and the incidence angle of 2° . The scanning step of the scintillation detector with a long plate collimator was 0.02° .

Results and discussion

Polarization curves in the tin electrolyte are depicted for various pH values (**Figure 1**). A significant cathodic shift of the tin reduction potential from approximately -0.28 V to -0.54 V with a change of pH from 2.2 to 8.0 was observed. According to the Nernst equation, a possible explanation could be either the change of the metal-complex character or the increase of the tin-complexes stability [17]. Simulation of the electrolyte speciation (Figure 2a) showed a changed distribution of Sn complexes in this pH region. In the weak acidic and neutral region, within the pH values of 4.0 and 7.0, Sn is mostly deposited from the $[\text{Sn}(\text{tart})_2]^{2+}$ complex. The observed shift in the Sn deposition potential in this pH region is caused by the increased stability of the $[\text{Sn}(\text{tart})_2]^{2+}$ complex [12]. On the other hand, in the more acidic pH region (pH values from 2.0 to 4.0), Sn is present in form of different complexes, such as $[\text{Sn}(\text{tart})_2]^{2+}$, $[\text{Sn}(\text{tart})]$, $[\text{SnCl}]^+$ or $[\text{SnCl}_2]$. The shift of the Sn reduction potential in this case is caused by the change of the concentrations of the various Sn complexes.

The anodic stripping voltammetries (ASV) were measured in the single metal Sn electrolyte with two different cathodic return potentials (-0.75 V and -1.25 V) at the initial electrolytes' pH with the value of 5.2 (Figure 3). For both return potentials, three stripping peaks (*A*, *B* and *C*) were observed. The peak *C* can be assigned to the passivation of Sn [18,19], peak *B* refers to the oxidation of Sn and thus its height depends on the amount of the reduced Sn [15]. The consecutive shoulder can be explained by the higher amount of

reduced Sn at the return potential of -1.25 V in comparison to the amount of Sn reduced at return potential of -0.75 V.

The Fe reduction potential was determined from the ASVs by changing the cathodic reverse potential (Figure 4). ASVs were performed in electrolytes with the pH values of 6.0 and 2.8. In the anodic branch, two peaks (*D* and *E*) were observed. The stripping peak *D* was detected, for the first time, in both pH values, when the electrode was polarized cathodically up to -0.85 V vs SHE. No stripping peak was detected with the cathodic return point of -0.75 V, which indicates, that the reduction potential of Fe lies between -0.75 and -0.85 V vs SHE (Figure 4). The potential of the peak *D* was shifted towards more positive values with the decrease of the electrolyte pH. Although the electrolyte speciation does not consider the possibility of oxidation of Fe²⁺ to Fe³⁺, it can indicate a possible mechanisms of Fe²⁺ reduction (Figure 2 b). At the pH value of 6.0, most of the Fe²⁺ ions should be present in the form of the [Fe(citr)]⁻ complex with the stability constant of 5.89 [14]. On the other hand, at the pH value of 2.8, Fe is predominantly reduced from the [Fe(SO₄)] (logK=2.8) and [FeH(citr)] with the stability constant, logK of 10.17 [14]. Therefore, it can be assumed, that the observed shift in the stripping peak *D* at the pH of 2.8, can be result of oxidation of Fe to [FeH(citr)]. Additionally, the peak *E* around +0.2 V was observed in single Fe electrolyte at the pH value of 6.0. Similar to peak *E*, the stripping peak *A* was detected in the single Sn electrolyte at the pH value of 5.2 (Figure 3). Analogous to the Fe stripping peak *D*, the potential of *E* was shifted towards more positive values when the electrolyte pH decreased to 2.8 (Figure 4). In our previous work [12] we have studied the mechanism of Fe-Sn electrodeposition from a similar electrolyte with tartrate as the single complexing agent. In the AVs of Fe, no additional stripping peaks such as *E* were observed. Moreover, the supporting electrolyte [12] did not have any anodic response.

This leads us to the assumption, that the origin of the peaks *A* and *E* could be in the oxidation of a citrate related species (Figure 2 d). However, for better understanding of the origin of stripping peaks *A* and *E*, more detailed analyses have to be performed.

For an alloy deposition of two different metals to occur, the difference between their standard reduction potentials E_0 should be less than 0.2 V [20]. If the alloy deposition of two metals is not possible, there is a need to shift their reduction potentials towards each other. Most common methods for bringing together two different reduction potentials are: changing the concentration of one of the metal species and thus altering its activity; changing the character and stability constants of the metal complexes; and usage of the selective surface active additives, which can increase the reduction overpotential of the more noble metal [20]. In the case of Sn^{2+} and Fe^{2+} , the difference between standard reduction potentials E_0 is -0.3 V [21]. A similar difference in the reduction potentials of Sn and Fe was estimated from the single metal electrolytes at the initial pH. For Sn at the pH of 5.2 the reduction potential was estimated to be around -0.45 V (Figure 1). For Fe the reduction potential at the initial electrolyte pH value of 6.0 was located between -0.75 and -0.85 V (Figure 4). The reduction potential of Sn at the lower pH is shifted towards more positive values (Figure 1) and with that, the difference between the reduction potentials of Fe and Sn is increasing. For this reason, the mixed Fe-Sn electrolyte with Fe to Sn ratio of 1:1 at the initial, non-adjusted pH value of 5.5 was chosen as optimal for Fe-Sn electrodeposition. Nevertheless, the mixed Fe-Sn electrolyte (pH~5.5) was changing the colour over time from light-yellow to orange-brownish, indicating the instability of the electrolyte. The current density transients were decreasing with every repetition. The value of the current density after 100 s of electrodeposition has changed from approximately -25 mAcm^{-2} at the first into half of its value in the third repetition (Figure 5 a). After 300 s of electrodeposition, the difference between the measured current

density in the first and the third repetition was one order of magnitude. Such massive changes in the current density after each experiment are confirming the instability of the electrolyte. The change of the electrolyte colour as well as its instability can be related to the oxidation of the ferrous ion and the creation of ferric hydroxide species [22,23]. Formation of hydroxides results in a reduced concentration of electroactive metal species and therefore also to the decrease of current density (Figure 5 a).

In order to suppress the oxidation of Fe^{2+} and the formation of hydroxides, the pH of the supporting electrolyte was adjusted to a value of around 3 before adding the Fe and Sn salts. This method of electrolyte preparation resulted in a Fe-Sn electrolyte with a Fe to Sn ratio of 1:1 at a pH of around 2.8. The colour of the electrolyte was light-green and did not change over time. The chronoamperometry results were reproducible (Figure 5). After 100 s of electrodeposition at -0.75 V, the recorded current densities were about -200 mAcm^{-2} , which is an order of magnitude higher than in the first measurement at the pH of 5.5 (Figure 5). The steep decrease in the recorded current densities over time indicates that the deposition at these conditions is not kinetically controlled and leads to a significant increase of the electrode's active area. Moreover, an increase in noise indicates a massive hydrogen evolution (Figure 5 b).

The change of the Fe-Sn (metal ion ratio of 1:1) electrolyte pH to 2.8 leads to an increase of its stability. On the other hand, it also causes the difference of the reduction potentials of Fe and Sn to increase to more than -0.4 V (Figure 1, Figure 4). In order to bring the reduction potentials closer together, the concentration of the more noble metal Sn was reduced. Electrolytes with Sn to Fe ratio of 1:1, 1:3 and 1:10 were tested. In these electrolytes, ASVs with different cathodic reverse potentials were performed in order to analyse the electrodeposited phases (Figure 6, Figure 7) and to determine the influence of the metal ion ratio in the electrolyte on the resulting electrodeposits. In the

thermodynamic phase diagram of Fe-Sn [3], in addition to the Sn phase and the solid solution of Fe-Sn, five intermetallic phases are found. Therefore, in ASVs, several stripping peaks were expected to be observed. The results of the ASVs with a cathodic polarization up to -1.25 V are depicted in Figure 6. Three stripping peaks (I, II, and III) were observed, independent of the electrolyte composition. Additionally, a small peak at the potential ~ 0.2 V was observed in all studied electrolyte compositions (Figure 6, Figure 7). Such a peak was also detected in the single Sn (peak *A*, Figure 3) and Fe (peak *E*, Figure 4) electrolytes. As it was already discussed above, the origin of this peak might be related to the oxidation of the citrate complexes, such as $[\text{H}_3(\text{citr})]$, $[\text{H}_2(\text{citr})]^-$ or $[\text{H}(\text{citr})]^{2-}$ (Figure 2 Figure 2 d). Therefore, this peak was not considered to be significant in the stripping analyses of Fe-Sn and will be a subject of further investigation. The peak heights of I, II and III depended on the metal ion ratios in the electrolyte. The peaks II and III were reduced in size with the decreased amount of Sn ions in the electrolyte. On the other hand, the height of peak I increased with higher concentrations of Fe ions (Figure 6). The peak Nr I (~ -0.4 V) appeared for the first time when the potential in the cathodic polarization reached -1.05 V vs SHE (Figure 7) and it was in good correlation to the stripping peak of Fe (Figure 6). This indicates that the peak Nr. I is probably related to the reduction of a Fe or Fe-rich intermetallic phase [24]. If both of the metals do not passivate in the investigated electrolyte, each stripping peak indicates a different intermetallic, intermediate or compound dissolution [24]. In the case of Fe, at the pH of 2.8, no passivation was observed (Figure 4). For Sn in the acidic citrate buffers (pH 3 and 4) a single anodic peak was observed, but it was also shown that it undergoes active dissolution-passivation process [25]. Therefore, it can be assumed that the three stripping peaks (*I*, *II* and *III*, Figure 6, Figure 7) belong to at least two different phases with the possibility, that one of them is a Fe or Fe-rich intermetallic phase [24,26].

A fast and an efficient way to perform electrodeposition with a range of current densities at once is a Hull cell. (Figure 8). Electrolytes with Sn to Fe ratio of 1:1 and 1:10 were selected for these experiments. In the case of the Sn-Fe electrolyte with an 1:1 metal ratio, massive grey dendrites were present over the whole current density range of the Hull cell (0.4- 40 mAcm⁻²) (Figure 8). The tree-like structure of the dendrites (Figure 9) indicates a fully diffusion controlled deposition [27]. With the increase of the Fe content in the electrolyte the morphology of the deposits slightly changed. The creation of the dendrites was suppressed below 10 mAcm⁻² (Figure 8) and their character changed from tree- to needle, carrot- like (Figure 9), which indicates the change of the deposition mechanism from purely diffusion controlled to mixed activation-diffusion controlled [27]. It was observed, that the electrodeposition from an electrolyte with Sn to Fe ratio of 1:1 follows normal deposition when samples with 19.84 at% of Fe were deposited at 40 mAcm⁻². Iron rich deposits (54.84 at %) were obtained from the electrolyte with an increased Fe content. Attempts to obtain homogeneous, smooth deposit were made by adding 1.6 mgL⁻¹ ABN additive into the iron rich electrolyte. In our previous studies [15], we have shown that, due to the ABN adsorption on the cathode in the chloride electrolytes, it acts as a very effective inhibitor and grain refiner for Sn. In the case of the Sn-Fe electrolyte, the presence of 1.6 mgL⁻¹ ABN significantly reduced the amount of dendrites on the Hull cell (Figure 8). On the other hand, in comparison to the iron rich electrolyte without ABN, the ratio of Sn to Fe in both the dendrites and the layer increased (Figure 9). A possible explanation is that with the adsorption of the ABN on the cathode both the hydrogen evolution and the Fe reduction are suppressed. Nevertheless, the exact role of ABN in the Fe-Sn chloride based electrolyte could be a part of further investigations.

The results from the X-ray analyses of the electrodeposited layers are compatible

with the findings from the ASVs. In all the studied electrolytes, three different phases were identified, namely: β -Sn and intermetallic phases FeSn_2 and Fe_5Sn_3 . The FeSn_2 phase is antiferromagnetic [3] and it was already electrodeposited by Chisholm et al.[11]. On the other hand the Fe_5Sn_3 phase exhibits ferromagnetic properties and is present in the thermodynamic phase diagram at temperatures above 1000 K [3]. The presence of the Fe_5Sn_3 phase was not influenced by the concentration of Fe in the electrolyte nor by the presence of ABN.

Conclusion

Due to their magnetic properties and low impact on human health and environment, Fe-Sn alloys are considered as one of the possible alternatives to nowadays used Fe based Ni, Co alloys. In the present work, the conditions for electrodeposition of Fe-Sn from a novel, green, ferrous chloride-based electrolyte were studied. It was observed, that due to the changing character of Sn complexes, the reduction potential of Sn depends on the electrolyte pH, while the reduction potential of Fe is independent of the pH value. Considering this dependency, the initial pH value of the mixed Fe-Sn electrolyte with the value of 5.5 was chosen as an optimum pH for Fe-Sn electrodeposition.

Nevertheless, the Fe^{2+} based electrolyte with a pH of 5.5 was unstable, changing colour from light-yellow to orange- brownish, indicating the formation of ferric hydroxides. As a result the recorded current density transients were decreasing with each repetition of the measurement. The stability of the electrolyte was improved by decreasing the pH to a value of 2.8. At this pH value the results of ASVs indicated the possibility to deposit at least two different phases, one of them containing iron.

The samples deposited from the electrolyte with a Sn to Fe ratio of 1:1 at the pH of 2.8 showed a regular deposition of Fe-Sn. At 40 mAcm^{-2} a deposit with 19.84 at% of

Fe were obtained. With the reduction of Sn concentration in the electrolyte, the content of Fe in the deposit increased to 54.84 at%. XRD results of the electrodeposited samples were compatible with ASVs. In both deposits the following phases were detected: β -Sn, and the intermetallics FeSn_2 and Fe_5Sn_3 . The Fe_5Sn_3 has a hexagonal structure and exhibits ferromagnetic properties and therefore, it is interesting for further investigation.

The Fe-Sn electrodeposition exhibits a complex interdependence of concentration, pH and deposition potentials. More detailed investigations of the Fe-Sn deposition mechanism could be performed in follow up studies.

Acknowledgements

This work was supported by the SELECTA (No. 642642) H2020-MSCA-ITN-2014 project. Authors would like to acknowledge Veronika Grman (Hirtenberger Engineering Surfaces) for performing SEM/EDX analyses and Werner Artner (X-ray Center, Vienna University of Technology) for the XRD analyses.

1. Izaki, M. Electrodeposition of Iron and Iron alloys. In *Modern electroplating*; 2011; pp. 309–326 ISBN 1118063147.
2. https://echa.europa.eu/candidate-list-table?p_p_id=disslists_WAR_disslistsportlet&p_p_lifecycle=1&p_p_state=normal&p_p_mode=view&p_p_col_id=column-1&p_p_col_pos=2&p_p_col_count=3&_disslists_WAR_disslistsportlet_javax.portlet.action=searchDissListsNo Accessible on 18.7.2019.
3. Giefers, H.; Nicol, M. High pressure X-ray diffraction study of all Fe–Sn intermetallic compounds and one Fe–Sn solid solution. *Journal of Alloys and Compounds* **2006**, *422*, 132–144, doi:10.1016/j.jallcom.2005.11.061.
4. Xiaowei, Zuo; Engang, W.; Huan, H.; Lin, Z.; Jicheng He Magnetic properties of Fe–49%Sn monotectic alloys solidified under a high magnetic field. *Journal of Alloys and Compounds* **2010**, *492*, 621–624.
5. Sales, B. C.; Saporov, B.; McGuire, M. A.; Singh, D. J.; Parker, D. S. Ferromagnetism of Fe₃Sn and alloys. *Scientific Reports* **2014**, *4*, 1–7, doi:10.1038/srep07024.
6. El-Sharif, M.; Chisholm, C. U.; Kuzmann, E.; Sziráki, L.; Stichleitner, S.; Homonnay, Z.; Süvegh, K.; Vértes, a. The structure and composition of novel electrodeposited Sn–Fe and Sn–Co–Fe alloys from a flow circulation cell system. *Hyperfine Interactions* **2009**, *192*, 1–12, doi:10.1007/s10751-009-9940-9.
7. Yelsukov, E. P.; Voronina, E. V.; Konygin, G. N.; Barinov, V. A.; Godovikov, S. K.; Dorofeev, G. A.; Zagainov, A. V Structure and magnetic properties of FeSn_x alloys obtained by mechanical milling. *Journal of Magnetism and Magnetic Materials* **1997**, *166*, 334–348.
8. System, I. I. T. S. Mechanically Alloyed Sn-Fe (-C) Powders as Anode Materials for Li-Ion Batteries. **1999**, *146*, 414–422.
9. Dionisio, P. H. Vasquez, A. Hallouche, B. Mosca Jr., D. H. Teixeira, S. R. Schreiner, W. H. Structural and Magnetic properties of iron-tin thin films. *Thin Solid Films* **1992**, *152–155*, doi:10.4028/www.scientific.net/SSP.233-234.666.
10. Haftek, E.; Tan, M.; Barnard, J. A. Microstructure and magnetic properties of ferromagnetic Fe-Sn alloy thin films. *Ultramicroscopy* **1992**, *47*, 400–407, doi:10.1016/0304-3991(92)90171-F.
11. Chisholm, C. U.; El-Sharif; Kuzmann, E.; Stichleitner, S.; Homonnay, Z.; Vertes, a. Electrodeposition of Sn-Fe alloys using gluconate electrolytes and X-ray diffractometry and Mossbauer studies of the deposits. *Materials Chemistry and Physics* **2010**, *120*, 558–565, doi:10.1016/j.matchemphys.2009.12.001.
12. Mrkonjić Zajkoska, S.; Dobročka, E.; Hansal, S.; Mann, R.; Hansal, W. E. G.; Kautek, W. Tartrate-Based Electrolyte for Electrodeposition of Fe–Sn Alloys. *Coatings* **2019**, *9*, 313, doi:10.3390/coatings9050313.
13. Petter, G. J. Visual MINDTEQ 3.1 2014.
14. Hyperquad Simulation and Speciation software.
15. Zajkoska, S.; Mulone, A.; Hansal, W.; Klement, U.; Mann, R.; Kautek, W. Alkoxyated β-Naphthol as an Additive for Tin Plating from Chloride and Methane Sulfonic Acid Electrolytes. *Coatings* **2018**, *8*, 79, doi:10.3390/coatings8020079.
16. Nohse, W. *The Hull cell*; Robert Draper LTD: Teddington, 1966;
17. Lowenheim, F. A. *Electroplating*; Technical Reference Publications LTD, 1995;
18. Šeruga, M.; Metikoš-Hukovič, M. Passivation of tin in citrate buffer solution. *Electrochimica Acta* **1992**, *334*, 223–240.
19. Tselesh, A. S. Anodic behaviour of tin in citrate solutions: The IR and XPS study

- on the composition of the passive layer. *Thin Solid Films* **2008**, *516*, 6253–6260, doi:10.1016/j.tsf.2007.11.118.
20. Brenner, A. *Electrodeposition of alloys, Principles and Practice, Volume I*; Academic Press, London, 1963;
 21. Bard, A. J. .; Parsons, R.; Jordan, J. *Standard potentials in aqueous solution*; 1st ed.; CRC Press, 1985;
 22. Silva, A. M. N.; Kong, X.; Parkin, M. C.; Cammack, R.; Hider, R. C. Iron(III) citrate speciation in aqueous solution. *Dalton Transactions* **2009**, 8616–8625, doi:10.1039/b910970f.
 23. Pham, A. N.; Waite, T. D. Oxygenation of Fe(II) in the presence of citrate in aqueous solutions at pH 6.0-8.0 and 25°C: Interpretation from an Fe(II)/citrate speciation perspective. *Journal of Physical Chemistry A* **2008**, *112*, 643–651.
 24. Jovic, V. D.; Zejnilovic, R. M.; Despica, A. .; Stevanovic, J. S. Characterization of electrochemically formed thin layers of binary alloys by linear sweep voltammetry. *Journal of Applied Electrochemistry* **1988**, *18*, 511–520, doi:10.1016/j.electacta.2012.12.053.
 25. Seruga, M.; Mtikos-Hukovic, M. Passivation of tin in citrate buffer solutions. *Journal of Electroanalytical Chemistry* **1992**, *334*, 223–240, doi:10.1016/0022-0728(92)80574-N.
 26. Morelock, R. J.; Sides, W. D.; Hu, Y.; Huang, Q. Electrochemical deposition and anodic stripping of PdZn bimetallic compound. *Journal of Electroanalytical Chemistry* **2018**, *815*, 8–15, doi:10.1016/j.jelechem.2018.03.003.
 27. Popov, K. I.; Djokić, S. S.; Nikolić, N. D.; Jović, V. D. *Morphology of Electrochemically and Chemically Deposited Metals*; 2016; ISBN 978-3-319-26071-6.

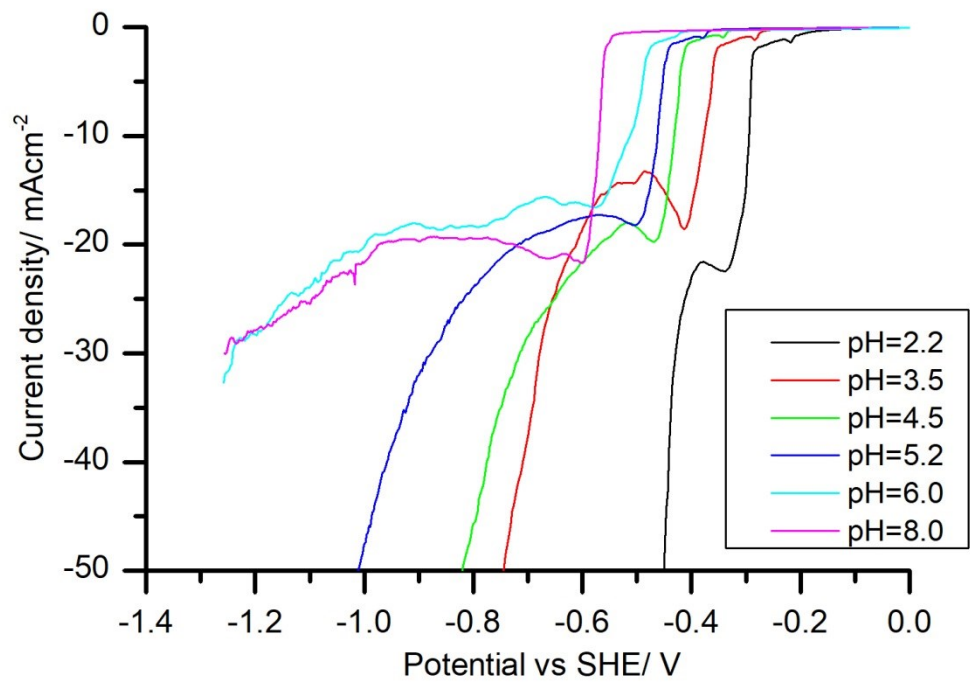


Figure 1: Dependence of the electrolyte pH on the cathodic polarisation behaviour of the Sn electrolyte. Measured with a scan rate of 5 mV/s.

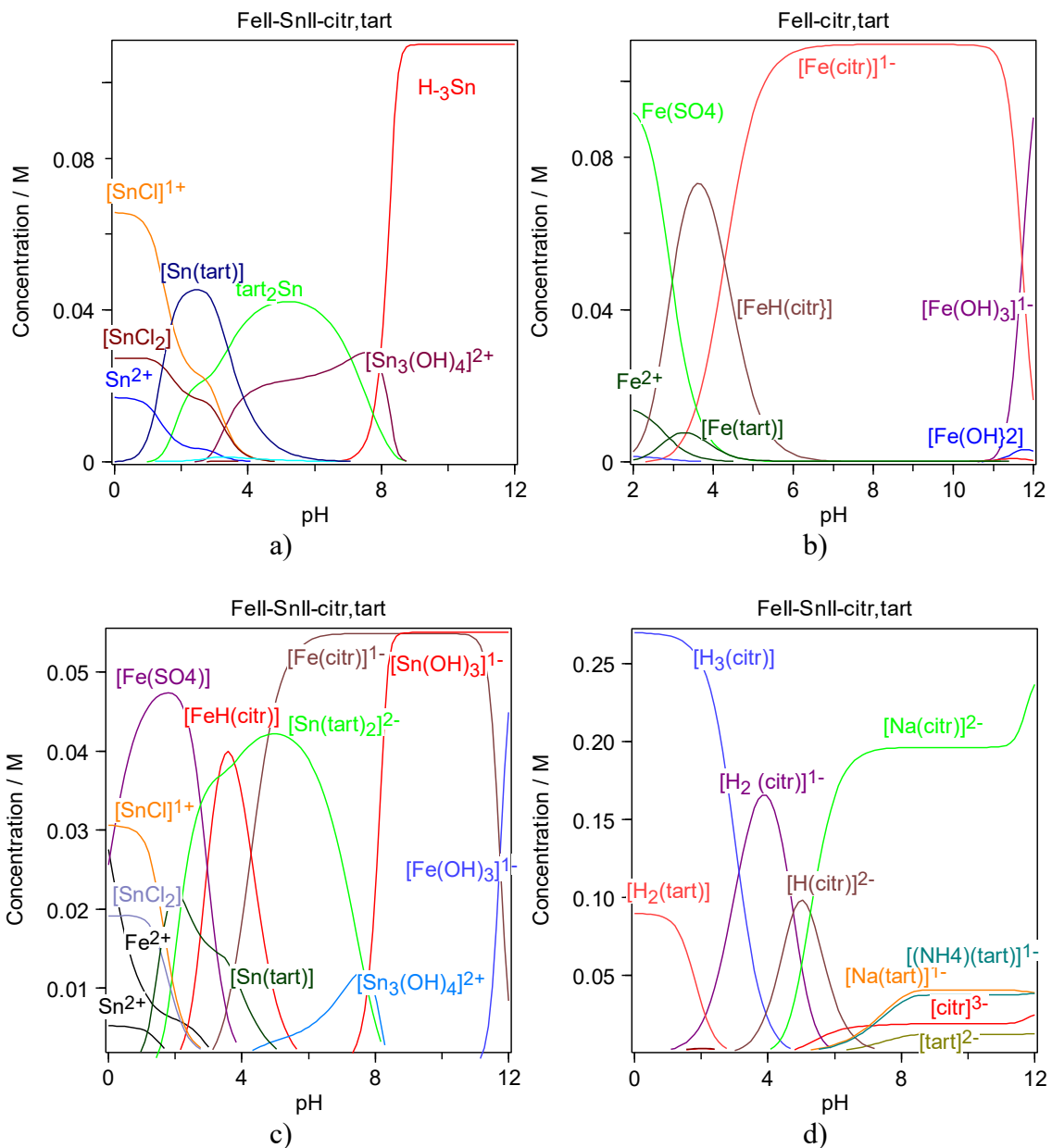


Figure 2: Electrolytes speciations: a) 0,11 M Sn single metal b) 0.11 M Fe single metal c) mixed Sn-Fe electrolyte with Sn: Fe ratio 1:1. Depicted are only Sn and Fe complexes. d) mixed Sn-Fe electrolyte with Sn: Fe ratio 1:1. Depicted are only citrate and tartrate non-metal complexes.

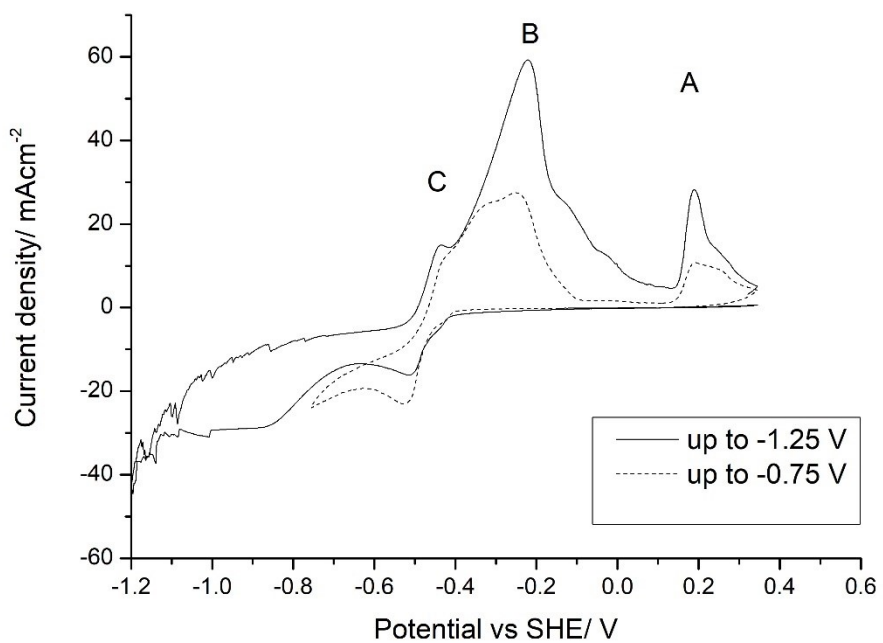


Figure 3: Anodic stripping voltammograms (ASV) measured in the 0.11 M Sn electrolyte, pH value of 5.2 with two different cathodic reverse potentials.

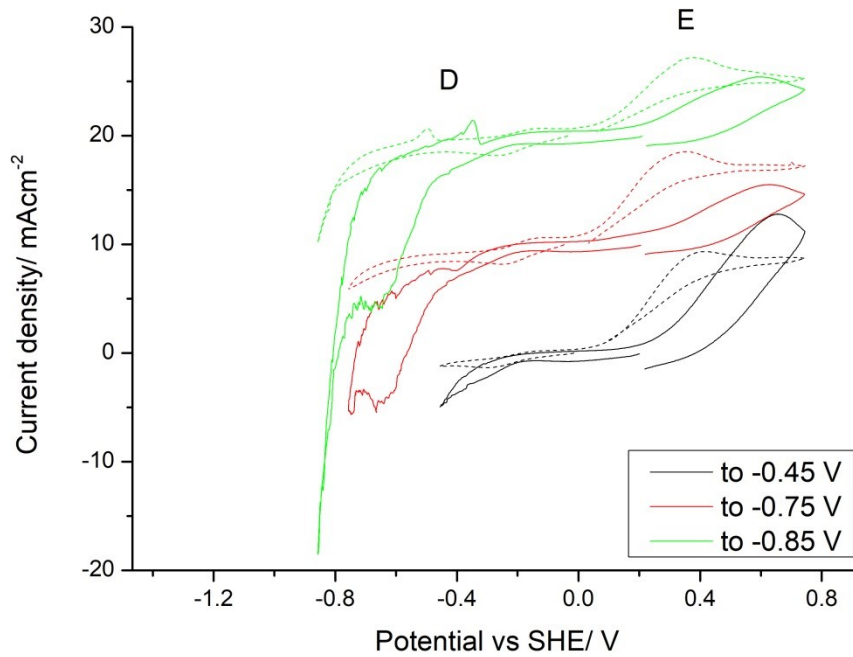


Figure 4: AVs with different cathodic reverse potential measured in the 0,11 M Fe electrolytes with the pH values of 6.0 (dashed) and 2.8 (full line). The anodic stripping peak D refers to the oxidation of Fe and was for the first time detected when the electrode was polarized cathodically up to -0.85 V vs SHE.

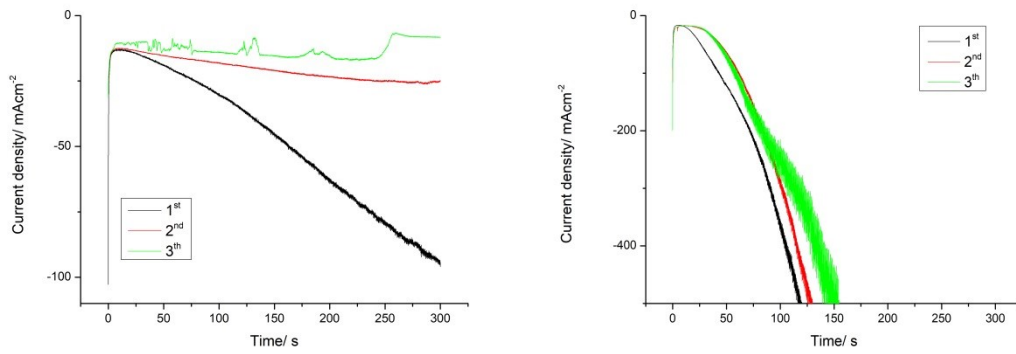


Figure 5: Current density transients recorded at the potential of -0.75 V in the Fe-Sn electrolyte with Fe to Sn metal ratio 1:1 and pH value of 5.5 (left) and 2.8 (right).

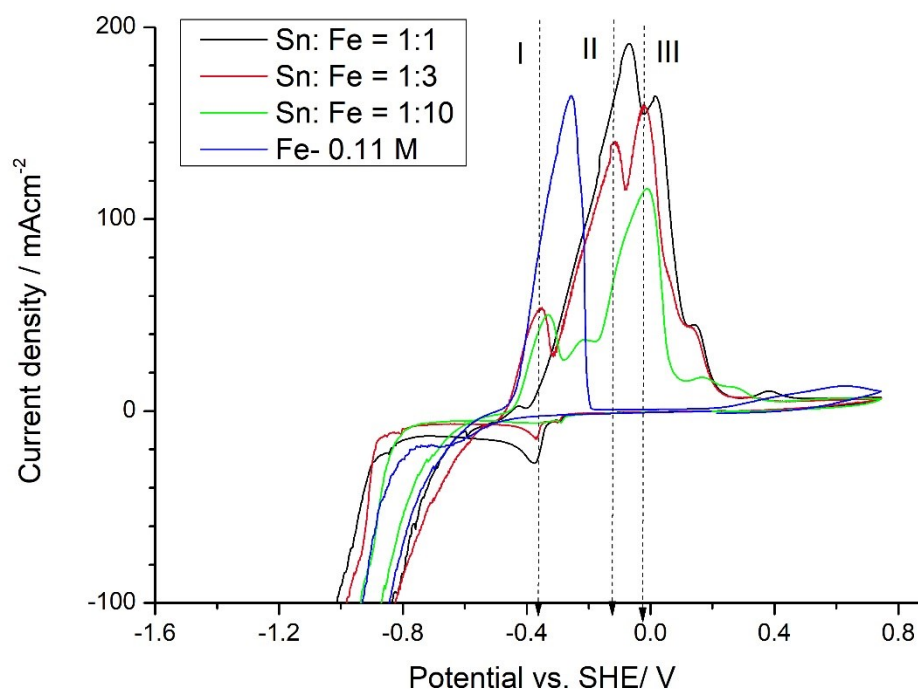


Figure 6: The influence of the Fe and Sn ion ratio in the electrolyte (pH~2.8) on the ASVs in comparison to the single metal Fe electrolyte. The Fe-Sn layers were polarized during the cathodic sweep up to the -1.25 V vs SHE. Consequently, anodic stripping up to +0.75 V vs SHE with the scan rate of 50 mV/s was performed. The vertical lines are marking the potentials of the stripping peaks in the electrolyte with Sn to Fe ratio 1:3 and cathodic reverse potential of -1.25 V.

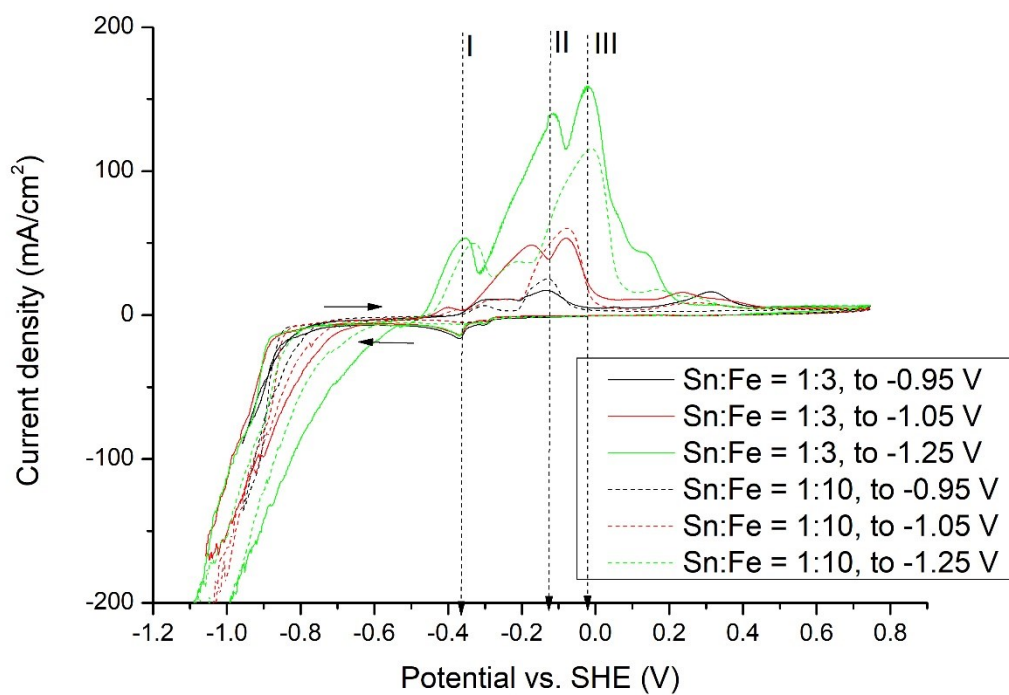


Figure 7: The influence of the cathodic reverse potential on the ASVs in the electrolytes with the electrolytes with the Sn:Fe ratio in the electrolyte 1:3 and 1:10. The vertical lines are marking the potentials of the stripping peaks in the electrolyte with Sn to Fe ratio 1:3 and cathodic reverse potential of -1.25 V.

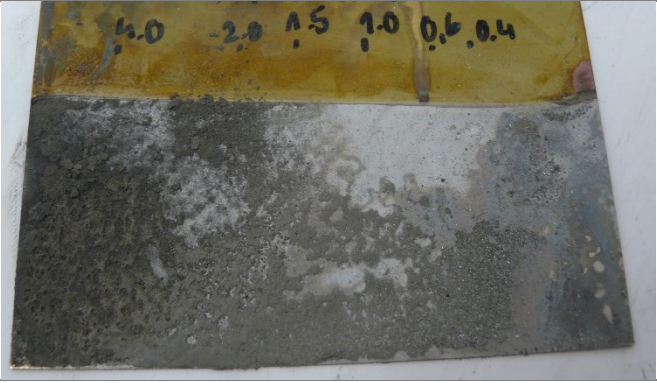
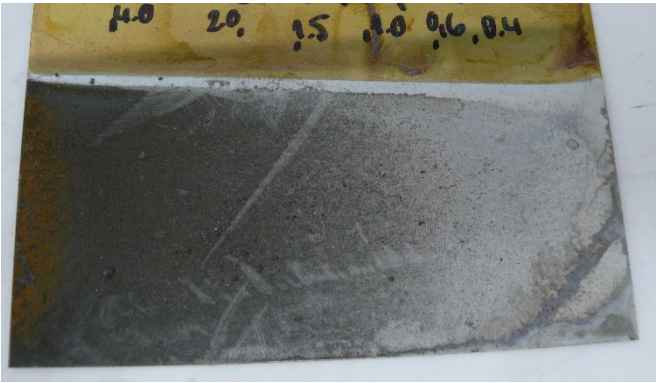
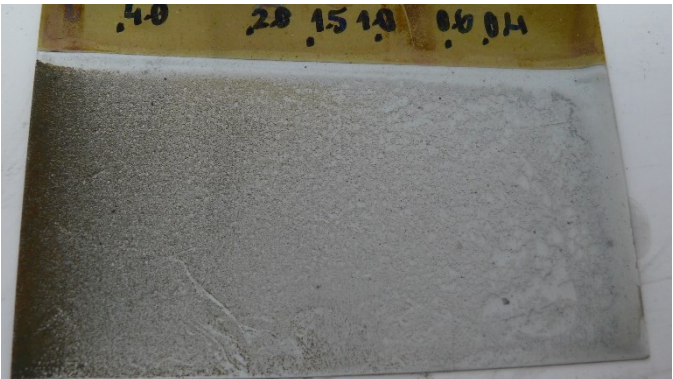
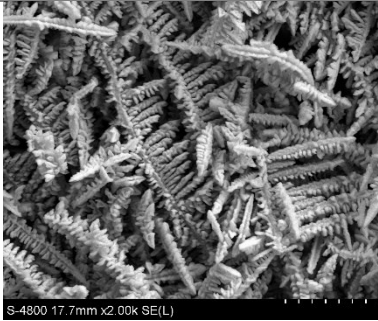
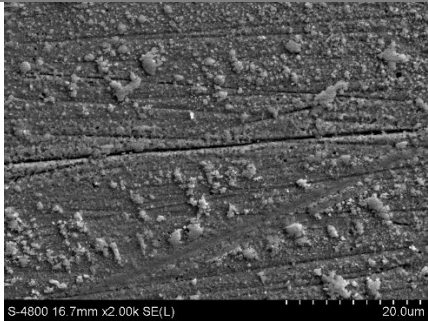
Sn: Fe	ABN (mgL ⁻¹)	
1:1	0	
1:10	0	
1:10	1.6	

Figure 8: Influence of the electrolyte composition on the character of the Hull cell deposits. Nominal current densities on the Hull cells are marked in the Adm^{-2} .

	ABN	Dendrites	Layer
Sn:Fe	(mgL ⁻¹)	EDX	EDX
	1)	SEM (2000x)	SEM (2000x)
		Sn:Fe (at %)	Sn:Fe (at %)
1:1	0	 96.57:3.43	 80.16:19.84

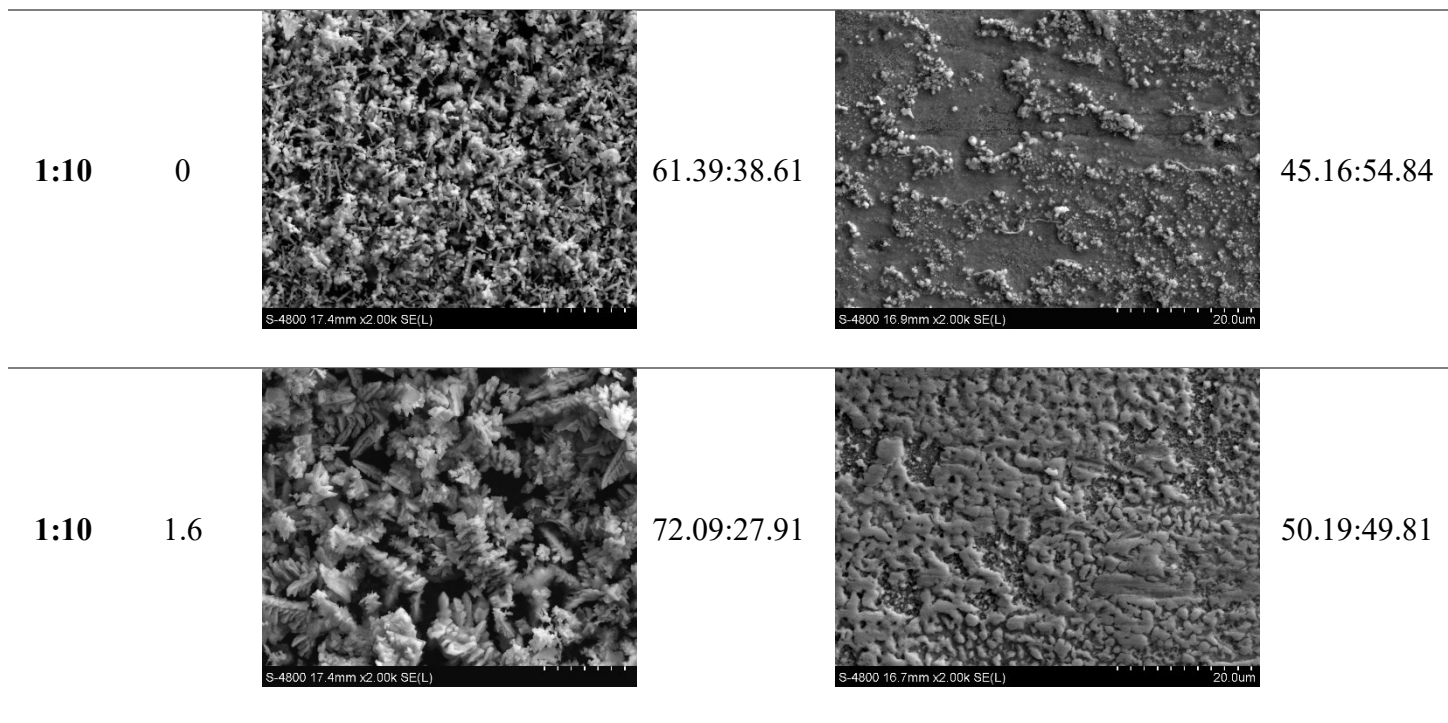


Figure 9: Topography images and stoichiometry of the electrodeposited dendrites and layers on the Hull cells at the nominal current density value of 40 mAcm^{-2} .

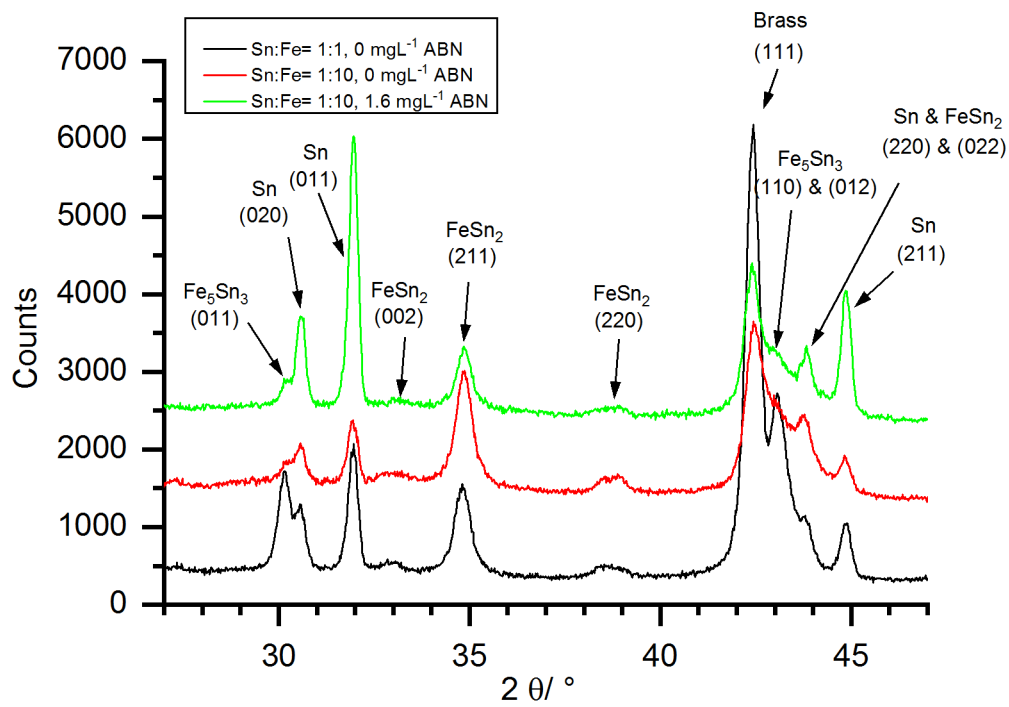


Figure 10: XRD diffractograms of the electrodeposited Sn-Fe from the electrolytes with Sn to Fe ions ratio 1:1 and 1:10, with and without the presence of ABN. The samples were obtained from a Hull cell deposition at a nominal current density value of 40 mAcm⁻².